Rod disc renewal occurs by evagination of the ciliary plasma membrane that makes cadherin-based contacts with the inner segment

Thomas Burgoyne[a,1], Ingrid P. Meschede[a,1], Jemima J. Burden[b], Maryse Bailly[a], Miguel C. Seabra[c,d], and Clare E. Futter[a,2]

[a]Institute of Ophthalmology, University College London, London, EC1V9EL, United Kingdom; [b]Laboratory for Molecular and Cell Biology, University College London, London, WC1E6BT, United Kingdom; [c]National Heart and Lung Institute, Imperial College, London, SW72AZ, United Kingdom; and [d]Centro de Estudos de Doenças Crónicas, NOVA Medical School/Faculdade de Ciências Médicas, Universidade Nova de Lisboa, 1169-056, Lisboa, Portugal

Edited by Theodore G. Wensel, Baylor College of Medicine, Houston, TX, and accepted by the Editorial Board November 17, 2015 (received for review June 5, 2015)

The outer segments of vertebrate rod photoreceptors are renewed every 10 d. Outer segment components are transported from the site of synthesis in the inner segment through the connecting cilium, followed by assembly of the highly ordered discs. Two models of assembly of discrete discs involving either successive fusion events between intracellular rhodopsin-bearing vesicles or the evagination of the plasma membrane followed by fusion of adjacent evaginations have been proposed. Here we use immuno-electron microscopy and electron tomography to show that rhodopsin is transported from the inner to the outer segment via the ciliary plasma membrane, subsequently forming successive evaginations that "zipper" up proximally, but at their leading edges are free to make junctions containing the protocadherin, PCDH21, with the inner segment plasma membrane. Given the physical dimensions of the evaginations, coupled with likely instability of the membrane cortex at the distal end of the connecting cilium, we propose that the evagination occurs via a process akin to blebbing and is not driven by actin polymerization. Disassembly of these junctions is accompanied by fusion of the leading edges of successive evaginations to form discrete discs. This fusion is topologically different to that mediated by the membrane fusion proteins, SNAREs, as initial fusion is between exoplasmic leaflets, and is accompanied by gain of the tetraspanin rim protein, peripherin.

rod photoreceptors | disc renewal | rhodopsin | protocadherin

Rod photoreceptors are specialized neurons of the vertebrate retina responsible for vision in dim light. The cylindrical outer segment (OS) contains ~1,000 stacked discontinuous membranous discs packed with the light-sensitive pigment rhodopsin. This contrasts with the cone OS, which consists of a series of evaginations of the plasma membrane that remain exposed to the extracellular space (1). OS constituents are synthesized in the inner segment (IS) and then transported to the OS via a nonmotile cilium (connecting cilium) that resembles the transition zone of the primary cilium. Because of the high metabolic demand of phototransduction, OS discs undergo daily renewal, whereby the tip (distal end) is shed and phagocytosed by the retinal pigment epithelium while new discs are formed at the base (proximal end) of the OS (2, 3). How these discs are generated and rhodopsin incorporated remains controversial. The evagination model proposes that the ciliary plasma membrane evaginates to form discs that are initially exposed to the extracellular space and then pinch off to form fully closed discs (4). In contrast, the fusion model proposes that discs originate from rhodopsin-containing vesicles, which undergo homotypic fusion to form new discs (5, 6). Conventional electron microscopic (EM) analyses of chemically fixed specimens have clearly shown discs open to the extracellular space at the base of the OS, supporting the evagination model (4, 7, 8). Furthermore, studies in amphibians have demonstrated that membrane impermeant dyes can stain discs at the base of the rod OS, indicating they are not enclosed by plasma membrane (9, 10). In contrast, EM analysis of frozen specimens has indicated the presence of vesicles apparently enclosed by plasma membrane at the base of the rod OS (5, 11, 12), supporting the fusion model, which predicts that rhodopsin-bearing vesicles must be transported through the connecting cilium or bud from the plasma membrane at the base of the OS. A recent study reported the existence of rhodopsin-bearing vesicles and tubules within the connecting cilium and at the base of the OS (13), but others have reported that most rhodopsin is transported on the ciliary plasma membrane (14). Furthermore, cryoelectron tomography failed to identify vesicles within the connecting cilium, but also presented data suggesting that nascent discs were enclosed within plasma membrane, which cannot be fully explained by either model (15).

In this manuscript, we show by immuno-EM that rhodopsin is transported primarily on the ciliary plasma membrane. By conventional EM and tomography, we demonstrate fusion of the open ends of adjacent nascent OS discs that have been formed by evaginations of the ciliary plasma membrane. Furthermore, we identify junctions between the IS and the OS that contain the photoreceptor-specific cadherin, PCDH21 (pr-CAD) (16), which may stabilize the ciliary membrane evagination and facilitate the formation of the remarkably ordered disk structure.

Results

Rhodopsin Is Transported on the Plasma Membrane of the Connecting Cilium. To determine whether rhodopsin-positive transport vesicles are present within the connecting cilium or the base of the OS, cryo-immunoEM of mouse retinal sections was performed using

Significance

Photoreceptors of the vertebrate retina contain specialized outer segments (OSs) where phototransduction begins. Rod OSs contain stacks of ordered membranous discs that undergo a daily renewal process essential for vision. Mechanisms underlying disc renewal are unclear. The biosynthetic machinery resides in the inner segment (IS), which is connected to the OS via a connecting cilium. Here, we use electron microscopy and tomography to show that the visual pigment, rhodopsin, traffics to the OS via the ciliary plasma membrane, which evaginates to form discs that are initially extracellularly exposed and that make novel contacts with the IS. Leading edges of adjacent evaginations then fuse to form discrete discs. Tomographic analysis leads us to propose a potential mechanism underlying the evagination process.

Author contributions: T.B., I.P.M., and C.E.F. designed research; T.B. and I.P.M. performed research; J.J.B. contributed new reagents/analytic tools; T.B., I.P.M., J.J.B., M.B., and C.E.F. analyzed data; and T.B., I.P.M., M.B., M.C.S., and C.E.F. wrote the paper.

The authors declare no conflict of interest.

This article is a PNAS Direct Submission. T.G.W. is a guest editor invited by the Editorial Board.

[1]T.B. and I.P.M. contributed equally to this work.

[2]To whom correspondence should be addressed. Email: c.futter@ucl.ac.uk.

This article contains supporting information online at www.pnas.org/lookup/suppl/doi:10.1073/pnas.1509285113/-/DCSupplemental.

antibodies to rhodopsin. In longitudinal sections, antibodies to the intradiscal N terminus and cytoplasmic C terminus of rhodopsin stained cytoplasmic vesicles in the IS, but in agreement with Wolfrum and Schmitt (14), within the connecting cilium, staining was confined to the ciliary plasma membrane (Fig. 1 *A* and *B*). Cross-sections through the connecting cilium, in which the microtubule doublets were clearly visible, also showed rhodopsin staining to be largely on the ciliary plasma membrane (Fig. 1*C*). Allowing for the potential distance (up to 25 nm) of the gold particle from the antigen because of the presence of antibodies/protein A, >90% of rhodopsin labeling localized to the plasma membrane, and no rhodopsin gold particles localized within the central lumen of the cilium (Fig. 1*D*). At the base of the OS, rhodopsin staining was confined to the OS plasma membrane and discs, and no rhodopsin-positive vesicles were observed (Fig. 1*B*). Together, these data indicate that the majority of rhodopsin is transported from the IS to the OS discs via the ciliary plasma membrane. We could discern particles within the ciliary lumen that had sticklike projections (Fig. 1*C*), which could correspond to the very small vesicles described by Chuang et al. (13) that were positive for an expressed rhodopsin horseradish peroxidase chimera. However, we never found rhodopsin staining on these particles. The only vesicular structures that labeled for rhodopsin were in the IS in close proximity to the base of the connecting cilium (Fig. 1*B*).

Developing Discs Are Evaginations of the Rod Plasma Membrane and Are Initially Extracellularly Exposed at the Perimeter of the OS. To further investigate the mechanism of OS disk formation, conventional EM was performed, allowing stronger fixation to enhance preservation of the forming OS discs. Ultrathin sections through the OS base showed up to 10 nascent discs (evaginations) clearly open to the extracellular space (Fig. 2*A*). Commonly, the axoneme was not in the section plane (as in Fig. 2), but its approximate position could be inferred, as the plasma membrane evaginates from the axoneme so the youngest (smallest) evagination highlights its position. 3D electron tomographic reconstructions allowed the continuity of the plasma membrane of successive lamellae to be unequivocally demonstrated (Fig. 2 *B*–*D* and Movies S1 and S2). Visualization in 3D emphasized the remarkable membrane remodeling that occurs as successive evaginations increase in width until they reach that of the OS. The tomographic slice through the IS:OS interface shown in Fig. 3*A* (Movie S3) again shows successive ciliary plasma membrane evaginations exposed to the extracellular space, but in this example, the axoneme is in the section plane. The base of successive ciliary plasma evaginations line up along the axoneme in a manner suggesting linkage to the axoneme, providing anchor points for evaginations.

Although our data agree with a number of studies showing nascent OS discs exposed to the extracellular space, they are at variance with others (5, 11, 12) that found vesicles at the base of the OS apparently enclosed in plasma membrane in frozen isolated neural retinae. We therefore analyzed high-pressure frozen samples of neural retinae and observed extensive damage that we suspected was sustained during the dissection of the retina before freezing (as the maximum tissue depth that can be frozen without risk of ice crystal damage is 200 μm). Chemical fixation of retinae dissected from the eyecup and tissue punches (Fig. S1) revealed that the OS had lost its close apposition, discs were disorganized, the periciliary ridge was often not visible, and the IS:OS interface was particularly disrupted compared with specimens in which the whole eye was immersed in fixative immediately after removal (Fig. S1). Vesicles apparently enclosed in plasma membrane were visible at the proximal end of the OS, as previously described in frozen specimens. We conclude therefore that immediate fixation in strong fixative before dissection is necessary to effectively

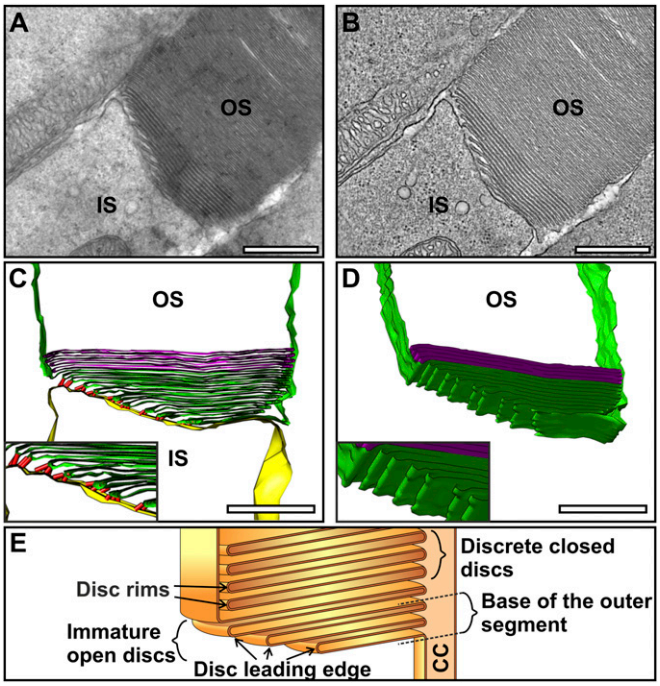

Fig. 2. Developing discs are evaginations of the rod photoreceptor plasma membrane. (*A*) Electron micrograph of a mouse rod photoreceptor IS and OS. (*B*) Slice from an electron tomogram generated from the corresponding photoreceptor *A*. (*C* and *D*) Model generated from the tomography data shows evaginations of the rod photoreceptor plasma membrane forming immature discs that are extracellularly exposed at the perimeter of the OS. Yellow represents the IS plasma membrane, green the developing discs, purple the mature discs, and red the junctions observed between the IS and OS plasma membrane. (*E*) Schematic diagram showing developing disk as evaginations of the rod photoreceptor plasma membrane with an exposed leading edge. (Scale bar, 500 nm.)

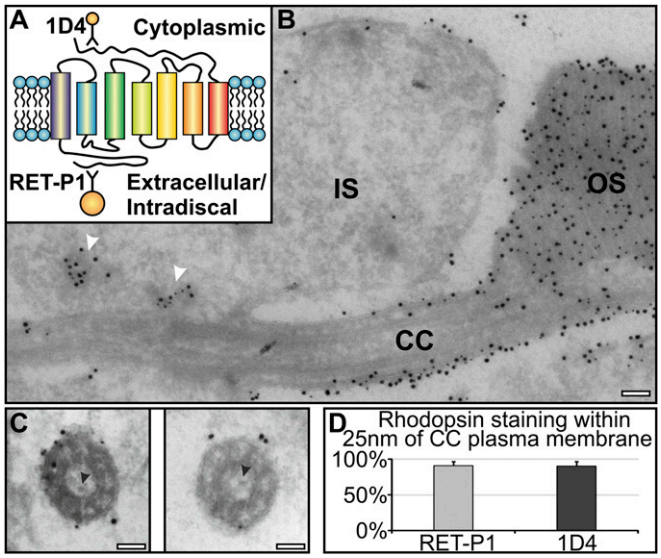

Fig. 1. Rhodopsin is transported to the newly forming discs via the connecting cilium plasma membrane. Retinal sections were labeled with two rhodopsin antibodies: 1D4 (10 nm gold) against the cytoplasmic and RET-P1 (15 nm gold) against the extracellular/intradiscal epitope. (*A*) Rhodopsin diagram showing the 1D4 and RET-P1 antibody epitope sites. (*B*) Note accumulation of rhodopsin-bearing vesicles (white arrowheads) in the IS at the base of the connecting cilium (CC) and rhodopsin confined to the plasma membrane within the CC and the discs within OS. (*C*) Cross-sections of the CC showing rhodopsin staining restricted to the plasma membrane. Black arrowheads indicate small vesicles with sticklike projections within the CC. (*D*) Percentage of rhodopsin labeling present on the ciliary plasma membrane. (Scale bar, 100 nm.)

CELL BIOLOGY

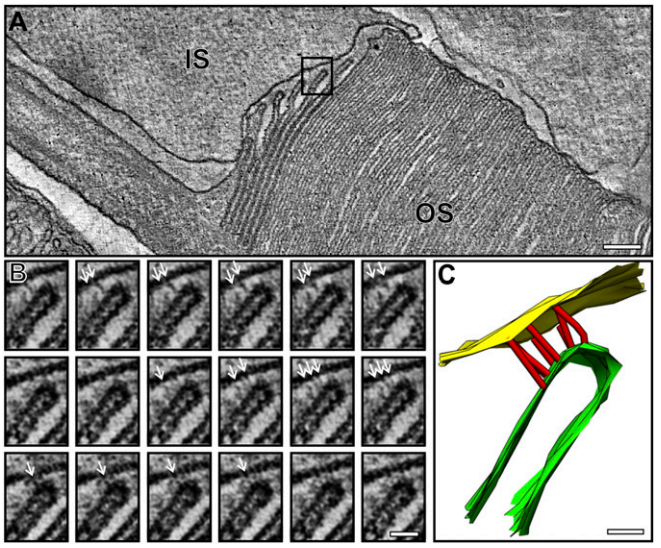

Fig. 3. Multiple junctions are present between the IS and the leading edge of developing discs. (*A*) A slice from a tomogram highlighting a region shown at a higher magnification in *B*. (*B*) Montage of slices from a tomogram showing junctions between the IS and the leading edge of a developing disk (white arrows). (*C*) Model generated from the tomography data, showing the spatial positioning of the junctions. Yellow corresponds to the IS, red represents junctions, and green the developing disk. (Scale bars, A, 100 nm; *B* and *C*, 25 nm.)

preserve the IS:OS interface and that vesiculation at the OS base occurs as a result of membrane disruption after dissection.

Interaction Between Adjacent Ciliary Plasma Membrane Evaginations and Between the Leading Edge of the Evaginations and the IS Plasma Membrane. Interestingly, adjacent plasma membrane evaginations are closely associated, appearing to be "zippered" from the base of the evagination at the axoneme but "unzippered" at the leading edge (Fig. 3*A*). This may leave the leading edge free for fusion. The leading edge of each evagination had an electron-dense cap on the extracellularly exposed face (clearly distinct from the cytoplasmically exposed rims at the axoneme between adjacent evaginations). Notably, these free leading edges of the evaginations that were not the full width of the OS were linked to the plasma membrane of the IS, and fibers could be discerned linking the opposing membranes (Fig. 2 *B* and *C* and Fig. 3). Tomography also allowed determination of the spatial positioning of the fibers, which appeared numerous in the depth of the reconstruction (Figs. 2*C* and 3 *B* and *C* and Movies S2 and S4).

OS Discs Are Closed by Fusion at the Leading Edge of Adjacent Evaginations. To generate discrete closed discs, the membranes of adjacent evaginations must fuse at the perimeter, allowing a continuous plasma membrane to then enclose discrete discs. Any given disk will be formed by progressive fusion between the leading edges of adjacent evaginations starting from the axoneme. Consistent with this progressive fusion, the tomographic data revealed instances in which the tomogram included regions in which, in some slices, the evaginations had fused. In Fig. 4, the axoneme was behind the plane of section (as evidenced by the small incisure in the central OS), so that evidence of disk fusion could be visualized on both sides of the OS section. Two regions (boxes in Fig. 4 *A* and *B*) that are open (to the extracellular space) in tomography slice A and closed in slice B are shown. Slice A is further than slice B from the axoneme (Fig. 4*C*). Successive slices of each region are shown in Fig. 4 *D* and *E* and clearly show fusion at the leading edge. 3D modeling of the boxed regions makes progressive fusion easier to visualize (Fig. 4 *F* and *G* and Movie S5).

Modulation of Disk Membrane Spacing Follows Disk Closure. An additional notable feature in disk maturation occurring after discrete disk development was a change in apparent membrane contrast in both EM micrographs and in the tomography data (Figs. 2 *A* and *B* and 4 *A* and *B*). Regions from the tomogram data containing both evaginations and discrete discs were extracted, and 3D rotational and translational mapping and subtomographic averaging were performed to enhance resolution and reduce noise. Distances between membranes from the averaged reconstructions were measured, and the difference in contrast was found to be a result of a change in membrane spacing (Fig. 5). The distance between adjacent zippered up plasma membrane evaginations was very small (1.4 nm), such that adjacent membranes appear as a wide, electron-dense band in lower-resolution images. Initially, after fusion between adjacent evaginations, the membranes that now surrounded the disk lumen remained very closely apposed, but after two to three discs, there was a change in spacing, such that the disk lumen widened to ~5.9 nm (Fig. 5*F*) and the membranes could be resolved even on lower-resolution images.

Cadherin-Containing Junctions Connect the Rims of Immature Discs to the Photoreceptor IS. The photoreceptor specific protocadherin, PCDH21, has been localized to the base of the OS and is required

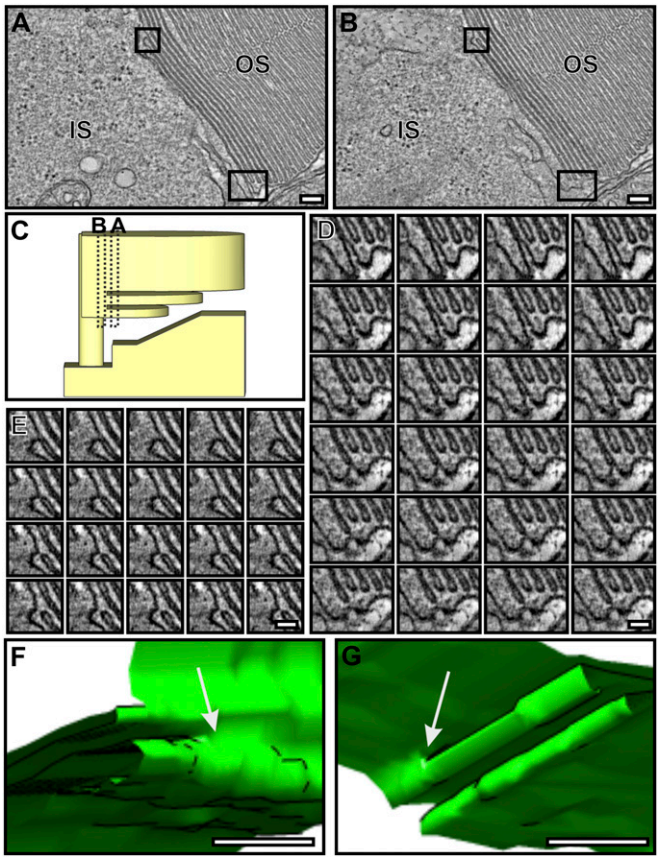

Fig. 4. Discrete discs are formed by the fusion of adjacent OS plasma membrane evaginations. (*A* and *B*) Two different slices from the same tomogram of a mouse rod photoreceptor. (*C*) The predicted position of the tomogram slices in *A* and *B*. The boxed regions in *A* show membrane that is open to the extracellular environment and fused in *B*. (*D* and *E* Montage of the tomogram slices corresponding to the boxed regions in *A* and *B*; the transition from open to closed membrane and the point of fusion between the adjacent plasma membrane to form a new disk is apparent. (*F* and *G*) Models generated from *D* and *E* showing the point of plasma membrane fusion in 3D. (Scale bars, *A* and *B*, 100 nm; *D* and *E*, 50 nm; *F* and *G*, 20 nm.)

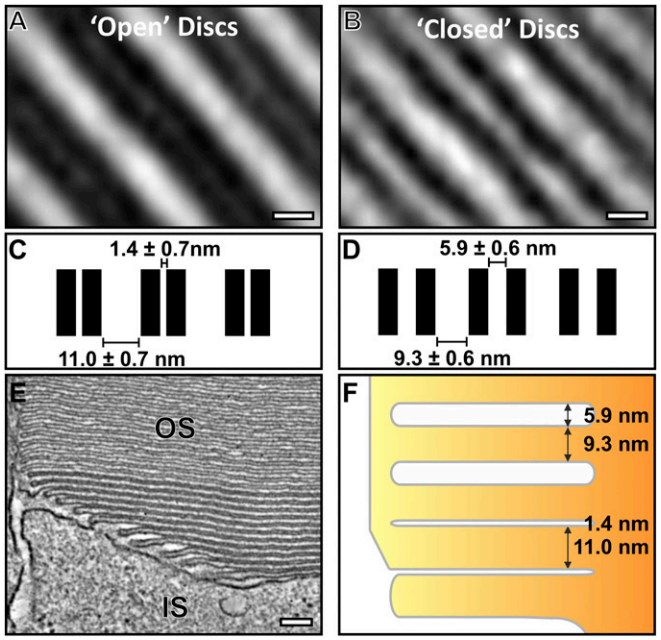

Fig. 5. As discs mature, a change in the membrane spacing occurs. (*A*) Slice from subtomographic average of developing "open" discs and (*B*) mature "closed" discs. Note that the open discs appear electron dense because of the small luminal space. (*C*) Measurements of the disk membrane spacing in developing open and (*D*) mature closed discs. (*E*) A slice from the tomographic data showing the apparent difference in disk spacing between developing and mature discs. (*F*) A corresponding schematic diagram highlighting the change in disk spacing as the discs mature. (Scale bars, *A* and *B*, 5 nm; *E*, 100 nm.)

for its structural integrity (16). Preembedding labeling confirmed the localization of PCDH21 to the base of the OS (Fig. 6*A*). To determine whether PCDH21 localized to the IS:OS junctions, we performed tomography on cryosections labeled with enhanced nanogold, allowing the junctions to be clearly visualized and modeled. As shown in the tomographic slice in Fig. 6*B*, the overlay in Fig. 6*C*, and Movie S6, almost all fibers connecting the tips of the plasma membrane evaginations at the base of the OS to the IS emanate from a PCDH21 gold particle on the OS (more examples in Fig. S2).

The Leading Edge of Ciliary Plasma Membrane Evaginations Lacks the Disk Protein, Peripherin. The tetraspannin protein, peripherin, localizes to disk rims (17, 18). Preembedding labeling showed peripherin localized to the disk rims at the base of the axoneme, but not to the leading edge of ciliary plasma membrane evaginations (Fig. 6*D*). After fusion to form discrete discs, peripherin localized to disk rims at the axoneme and the OS perimeter, with some staining on the intervening disk membranes.

Absence of the SNARE Proteins, Syntaxin 3 and Munc-18, from the Base of the OS. The previously reported presence of syntaxin 3 and Munc18 in the OS (19) and the described role for syntaxin 3 in fusion of rhodopsin-bearing vesicles at the base of the OS (6) lead us to localize these SNARE proteins by preembedding labeling. Syntaxin 3 and Munc-18 labeling was confined to the plasma membrane of the IS and periciliary ridge (Fig. 6 *E* and *F*) and was largely undetectable in the base of the OS.

Discussion

The exquisitely ordered structure of the light-sensitive photoreceptor OS discs was first described >50 y ago, yet the mechanisms regulating disk biogenesis remain a subject of debate. Interference with any part of this highly ordered process likely causes gross changes in OS morphology, making it difficult to dissect the molecular regulation of individual steps. Furthermore, any genetic manipulation that affects rhodopsin transport, which constitutes >50% of the rod OS, indirectly affects disk biogenesis. However, the huge amount of photoreceptor membrane synthesized/day uniquely allows biosynthetic transport to be visualized in a single snapshot, using the combination of immunogold and conventional EM and electron tomography we report here.

Our demonstration that >90% of rhodopsin molecules are transported to the OS via the ciliary plasma membrane is in agreement with the data of Wolfrum and Schmitt (14). It contrasts, however, with that of Chuang et al. (13), who, by immunogold EM, reported rhodopsin staining within the ciliary lumen, as well as on the plasma membrane, and also found vesicles and tubules within the ciliary lumen, some of which were positive for an expressed rhodopsin horseradish peroxidase chimera. We did observe small particles within the lumen of the cilium, and so cannot rule out the possibility that membrane transport could occur through the lumen. However, these particles did not stain for rhodopsin, despite our staining of the surface of ultrathin cryosections (with C- and N-terminal rhodopsin antibodies), providing accessibility to the lumen of the cilium. This indicates that at least the majority of rhodopsin is transported on the ciliary plasma membrane. Consistently, components of the intraflagellar transport complexes that link ciliary cargo to the microtubule cytoskeleton (20, 21) and the anterograde motor, kinesin II (22, 23), have been implicated in ciliary transport of rhodopsin.

We have clearly shown in multiple tomograms that the nascent discs at the base of the OS are exposed to the extracellular space, and so are formed by evaginations of the plasma membrane, in agreement with Steinberg et al. (4). How has electron microscopy of the base of the OS convincingly shown plasma membrane evaginations (4, 7, 8) in some studies and vesicles apparently enclosed by plasma membrane in others (5, 12)? We have shown that the method of specimen preparation is key to preservation of the IS:OS interface. The dissection of the neural retina from the eyecup typically performed before cryopreservation of the retina can lead to membrane vesiculation at the base of the OS. Immediate fixation of the whole eye preserves the IS:OS interface, and a failure to do this may underlie some of the differences in reported membrane organization that have led to controversy in this field. Our tomographic reconstructions also show that

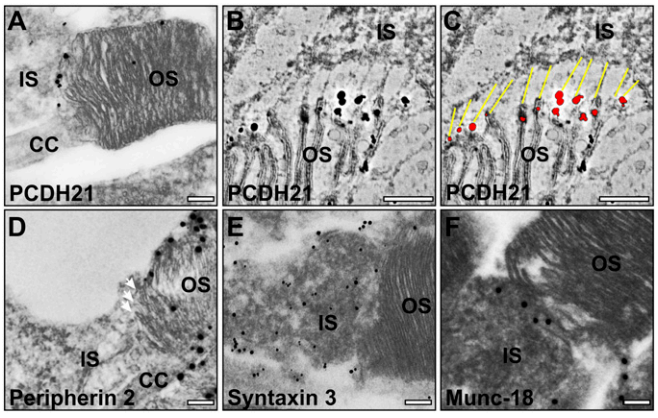

Fig. 6. Immunogold labeling of proteins involved in rod photoreceptor disk development. (*A*–*C*) Photoreceptor-specific cadherin (PCDH21) labels the junctions between the developing discs and the IS. (*B* and *C*) Slices from a tomogram where junctions are visible between the IS and OS and are highlighted in yellow (*C*), emanating from PCDH21 gold labeling shown in red. (*D*) Peripherin 2 is present on the rims of all discs but is excluded from the tips of the developing disk (white arrows). (*E*) Syntaxin 3 is present on the plasma membrane of the IS and is likely to be involved in membrane recruitment, but is absent from the OS. (*F*) Munc-18 labeling is predominantly in the IS. (Scale bars, 200 nm.)

successive ciliary plasma membrane evaginations fuse to form discrete discs. This progressive disk closure from the axoneme could lead to the nascent discs appearing to be enclosed by plasma membrane, as previously described in both frozen and chemically fixed preparations (13, 15), depending upon the position of the axoneme within the section plane and the section orientation.

Topologically, the evagination process is akin to the lamellipod extension driven by actin polymerization (24), and inhibition of actin polymerization has been shown to cause the formation of a reduced number of enlarged OS discs (25–28). However, the evaginations that lead to rod disk biogenesis have a depth of 11 nm, in contrast to a minimum of 100 nm for lamellipodia, which contain a network of multiple layers of actin filaments (each ∼10 nm in diameter), as well as a large number of cytoskeletal and signaling proteins (24, 29). The limited dimensions of the ciliary plasma membrane evaginations therefore make it highly unlikely they are driven by actin polymerization. An alternative explanation for the ciliary plasma membrane evagination is a form of blebbing, a process driven not by actin polymerization but by localized detachment of the plasma membrane from the cortical actin cytoskeleton, which leads to rapid protrusion of the plasma membrane driven by the cell's internal hydrostatic pressure. Although most commonly associated with cell injury, blebbing is also part of physiological processes such as cytokinesis and motility (30). Destabilization of the membrane cortex with cytochalasin D has been shown to result in the formation of fewer, but larger, blebs in HeLa cells (31), reminiscent of the overgrown discs caused by cytochalasin treatment in the eye (25–28). The accumulation of newly synthesized rhodopsin, but not a rod cGMP-gated plasma membrane channel, in the overgrown cytochalasin-induced discs, suggests F-actin may coordinate the postevagination phase of assembly of discrete discs separate from the plasma membrane (28).

The extraordinary configuration of the membrane/cortex links at the IS:OS interface (modeled in Fig. 7) could provide an environment that favors the formation of flattened blebs. The narrow connecting cilium is linked extracellularly to the IS periciliary ridge (32, 33) by fibers containing components of the Usher Syndrome (Ush) protein network, also found in the ankle links of inner ear hair cell cilia (33–35). The cytoplasmic face of the connecting cilium plasma membrane is linked to microtubules via intraflagellar transport particles. These extracellular and intracellular links must detach at the base of OS, which, together with the continued arrival of new membrane via the connecting cilium, could create membrane tension conditions favorable for blebbing. In addition, strong confinement, shown to promote blebbing (36), is provided by the narrow space between the periciliary ridge and the OS. The disruption of such a peculiar configuration after mechanical stress (e.g., during sample preparation for cryopreservation) could result in uncontrolled blebbing and vesiculation.

The base of successive evaginations line up adjacent to the axoneme, suggesting they are tethered to the axonemal microtubules, providing anchor points for successive evaginations. The membrane of each new evagination interacts proximally with the neighboring previously formed evagination (giving the zippering appearance), and the free leading edge of each evagination makes junctions with the top of the periciliary ridge. Together, these interactions may regulate bleb shape and inhibit bleb retraction. The junctions between the leading edge of the evaginations and the IS contain the protocadherin PCDH21. Consistent with a role for PCDH21 in disk development, its deletion in mice causes the development of disorganized OS discs (16).

Cadherins typically interact with cadherins of the same family on neighboring cells, but our identification of junctions between the IS and OS (i.e., different parts of the same cell) demonstrates an interesting parallel with the stereocilia of the hair cells of the inner ear. The protocadherin, PCDH15, binds the cadherin, CDH23, at the tip links of the stereocilia (37). So whereas ciliary plasma membrane junctions with the side of the IS periciliary ridge resemble the ankle links of the stereo cilia, the evaginating ciliary plasma membrane junctions with the top of the IS periciliary ridge may resemble the tip links of the stereo cilia. The binding partner of PCDH21 on the IS remains to be identified. It is not clear whether or not PCDH15 is on the IS (38, 39), but members of the USH1 network, which include PCDH15 and CDH23, are possible candidates. The presence of cadherin-containing links between the tips of the nascent discs and the IS provides significant further evidence the discs are plasma membrane evaginations, rather than cytoplasmic vesicles, corroborating the evagination model rather than the fusion model.

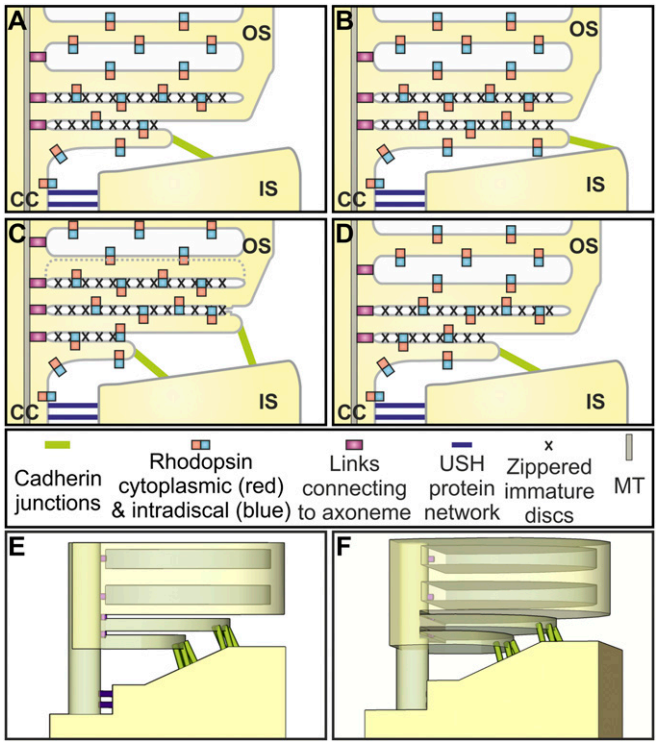

Fig. 7. Model of maturation of rod photoreceptor discs. (*A–D*) Schematic showing the rhodopsin-containing plasma membrane of the connecting cilium that is linked to the side of the periciliary ridge by the USH protein network. The evaginating rhodopsin-containing membrane zippers up with neighboring evaginations proximally, leaving the leading edge free to interact with the top of the periciliary ridge via PCDH21-containing junctions. Discs at the base of the evaginations are anchored to the axoneme. The leading edges of neighboring evaginations fuse to form closed discs, accompanied by disassembly of the PCDH21-containing junctions and followed by change in membrane spacing to generate discs with a greater depth. (*E* and *F*) 3D models of the base of the OS showing cadherin junctions between developing discs and the periciliary ridge of the IS.

The evagination and fusion models of rod disk biogenesis predict very different regulatory machineries, as the fusion model predicts SNARE-mediated fusion between intracellular rhodopsin-containing vesicles, whereas the evagination model predicts fusion between extracellular plasma membrane leaflets. The SNAREs, Syntaxin 3 and Munc-18, have been localized to the IS, cilium, and OS, with syntaxin 3 localized primarily to the OS base (6, 19), and they have a role in the fusion of rhodopsin carriers with the plasma membrane of the IS (40). Syntaxin 3 has also been proposed to regulate vesicle fusion with the forming discs at the base of the OS in a complex with rhodopsin and SARA (6). However, we found that whereas syntaxin 3 and Munc-18 are on the IS plasma membrane apposing the forming OS discs, they are largely absent from the OS base. Syntaxin 3 and Sara may have indirect roles in OS disk biogenesis by mediating rhodopsin transport to the cilium.

Fusion of adjacent evaginated membranes to form closed discs must be accompanied by disassembly of the PCDH21-based

junctions. The ectodomain of PCDH21 is subject to proteolytic cleavage (41), providing a potential way to couple PCDH21 junctional disassembly with closed disk formation. Fusion between the leading edges of adjacent evaginations is accompanied by assembly of the peripherin-containing disk rim. We found that although peripherin was present at the base of all ciliary plasma membrane evaginations at the axonemal side, it was absent from the leading edges of the ciliary plasma membrane evaginations, consistent with their reverse topology. However, the presence of peripherin staining on the newly formed rims after disk closure suggests peripherin recruitment accompanies fusion between the leading edges of adjacent evaginations. Interestingly the zippering between the membranes of neighboring evaginations is lost in the mature discs after closure, suggesting conformational change in interacting proteins after loss of exposure to the extracellular milieu.

We have unequivocally demonstrated that mouse rod OSs are renewed by evagination of the ciliary plasma membrane, followed by fusion between the leading edges of neighboring evaginations. Before fusion, the leading edges of evaginations make PCDH21-containing contacts with the IS plasma membrane that may stabilize and control the evagination. Establishing the membrane traffic steps required for disk renewal has major implications for its molecular regulation and will aid in the understanding of how defects in membrane traffic can lead to progressive the OS degeneration that is a feature of many retinal degenerative diseases.

Materials and Methods

Eyes from C57BL6 mice were processed for conventional EM, tomography, cryo-immunoEM, and preembedding labeling, as described in detail, with information about the antibodies, staining methods, and software used, in the *SI Materials and Methods*. Mice used in this study were treated in accordance with Home Office guidance rules, adhering to the Association for Research in Vision and Ophthalmology Statement for the Use of Animals in Ophthalmic and Vision Research.

Note Added in Proof. Since final review and acceptance of this study Ding et al. (42) have presented data supporting a membrane evagination mechanism for rod disc renewal and Volland et al. (43) have presented an invagination, followed by evagination, model from analysis of the 3D organization of nascent rod discs.

ACKNOWLEDGMENTS. We thank Mike Powner for providing mouse eyes and Peter Munro and Matt Hayes from the Institute of Ophthalmology Imaging Facility for technical assistance. This work was funded by grants from the Wellcome Trust (093445) and RP Fighting Blindness (GR577).

1. Eckmiller MS (1987) Cone outer segment morphogenesis: Taper change and distal invaginations. *J Cell Biol* 105(5):2267–2277.
2. Young RW, Bok D (1969) Participation of the retinal pigment epithelium in the rod outer segment renewal process. *J Cell Biol* 42(2):392–403.
3. Young RW (1976) Visual cells and the concept of renewal. *Invest Ophthalmol Vis Sci* 15(9):700–725.
4. Steinberg RH, Fisher SK, Anderson DH (1980) Disc morphogenesis in vertebrate photoreceptors. *J Comp Neurol* 190(3):501–508.
5. Obata S, Usukura J (1992) Morphogenesis of the photoreceptor outer segment during postnatal development in the mouse (BALB/c) retina. *Cell Tissue Res* 269(1):39–48.
6. Chuang JZ, Zhao Y, Sung CH (2007) SARA-regulated vesicular targeting underlies formation of the light-sensing organelle in mammalian rods. *Cell* 130(3):535–547.
7. Kinney MS, Fisher SK (1978) The photoreceptors and pigment epithelium of the larval Xenopus retina: Morphogenesis and outer segment renewal. *Proc R Soc Lond B Biol Sci* 201(1143):149–167.
8. Besharse JC, Hollyfield JG, Rayborn ME (1977) Turnover of rod photoreceptor outer segments. II. Membrane addition and loss in relationship to light. *J Cell Biol* 75:507–527.
9. Laties AM, Bok D, Liebman P (1976) Procion yellow: A marker dye for outer segment disc patency and for rod renewal. *Exp Eye Res* 23(2):139–148.
10. Kaplan MW, Iwata RT, Sterrett CB (1990) Retinal detachment prevents normal assembly of disk membranes in vitro. *Invest Ophthalmol Vis Sci* 31(1):1–8.
11. Usukura J, Obata S (1995) Morphogenesis of Photoreceptor Outer Segments in Retinal Development. *Prog Retin Eye Res* 15:113–125.
12. Miyaguchi K, Hashimoto PH (1992) Evidence for the transport of opsin in the connecting cilium and basal rod outer segment in rat retina: Rapid-freeze, deep-etch and horseradish peroxidase labelling studies. *J Neurocytol* 21(6):449–457.
13. Chuang JZ, Hsu YC, Sung CH (2015) Ultrastructural visualization of trans-ciliary rhodopsin cargoes in mammalian rods. *Cilia* 4:4.
14. Wolfrum U, Schmitt A (2000) Rhodopsin transport in the membrane of the connecting cilium of mammalian photoreceptor cells. *Cell Motil Cytoskeleton* 46(2):95–107.
15. Gilliam JC, et al. (2012) Three-dimensional architecture of the rod sensory cilium and its disruption in retinal neurodegeneration. *Cell* 151(5):1029–1041.
16. Rattner A, et al. (2001) A photoreceptor-specific cadherin is essential for the structural integrity of the outer segment and for photoreceptor survival. *Neuron* 32(5):775–786.
17. Arikawa K, Molday LL, Molday RS, Williams DS (1992) Localization of peripherin/rds in the disk membranes of cone and rod photoreceptors: Relationship to disk membrane morphogenesis and retinal degeneration. *J Cell Biol* 116(3):659–667.
18. Molday RS, Hicks D, Molday L (1987) Peripherin. A rim-specific membrane protein of rod outer segment discs. *Invest Ophthalmol Vis Sci* 28(1):50–61.
19. Kwok MC, Holopainen JM, Molday LL, Foster LJ, Molday RS (2008) Proteomics of photoreceptor outer segments identifies a subset of SNARE and Rab proteins implicated in membrane vesicle trafficking and fusion. *Mol Cell Proteomics* 7(6):1053–1066.
20. Keady BT, Le YZ, Pazour GJ (2011) IFT20 is required for opsin trafficking and photoreceptor outer segment development. *Mol Biol Cell* 22(7):921–930.
21. Pazour GJ, et al. (2002) The intraflagellar transport protein, IFT88, is essential for vertebrate photoreceptor assembly and maintenance. *J Cell Biol* 157(1):103–113.
22. Marszalek JR, et al. (2000) Genetic evidence for selective transport of opsin and arrestin by kinesin-II in mammalian photoreceptors. *Cell* 102(2):175–187.
23. Trivedi D, Colin E, Louie CM, Williams DS (2012) Live-cell imaging evidence for the ciliary transport of rod photoreceptor opsin by heterotrimeric kinesin-2. *J Neurosci* 32(31):10587–10593.
24. Ridley AJ (2011) Life at the leading edge. *Cell* 145(7):1012–1022.
25. Williams DS, Linberg KA, Vaughan DK, Fariss RN, Fisher SK (1988) Disruption of microfilament organization and deregulation of disk membrane morphogenesis by cytochalasin D in rod and cone photoreceptors. *J Comp Neurol* 272(2):161–176.
26. Vaughan DK, Fisher SK (1989) Cytochalasin D disrupts outer segment disc morphogenesis in situ in rabbit retina. *Invest Ophthalmol Vis Sci* 30(2):339–342.
27. Hale IL, Fisher SK, Matsumoto B (1996) The actin network in the ciliary stalk of photoreceptors functions in the generation of new outer segment discs. *J Comp Neurol* 376(1):128–142.
28. Nemet I, Tian G, Imanishi Y (2014) Submembrane assembly and renewal of rod photoreceptor cGMP-gated channel: Insight into the actin-dependent process of outer segment morphogenesis. *J Neurosci* 34(24):8164–8174.
29. Insall RH, Machesky LM (2009) Actin dynamics at the leading edge: From simple machinery to complex networks. *Dev Cell* 17(3):310–322.
30. Charras GT (2008) A short history of blebbing. *J Microsc* 231(3):466–478.
31. Charras GT, Hu CK, Coughlin M, Mitchison TJ (2006) Reassembly of contractile actin cortex in cell blebs. *J Cell Biol* 175(3):477–490.
32. Peters KR, Palade GE, Schneider BG, Papermaster DS (1983) Fine structure of a periciliary ridge complex of frog retinal rod cells revealed by ultrahigh resolution scanning electron microscopy. *J Cell Biol* 96(1):265–276.
33. Maerker T, et al. (2008) A novel Usher protein network at the periciliary reloading point between molecular transport machineries in vertebrate photoreceptor cells. *Hum Mol Genet* 17(1):71–86.
34. Michalski N, et al. (2007) Molecular characterization of the ankle-link complex in cochlear hair cells and its role in the hair bundle functioning. *J Neurosci* 27(24):6478–6488.
35. McGee J, et al. (2006) The very large G-protein-coupled receptor VLGR1: A component of the ankle link complex required for the normal development of auditory hair bundles. *J Neurosci* 26(24):6543–6553.
36. Liu YJ, et al. (2015) Confinement and low adhesion induce fast amoeboid migration of slow mesenchymal cells. *Cell* 160(4):659–672.
37. Kazmierczak P, et al. (2007) Cadherin 23 and protocadherin 15 interact to form tip-link filaments in sensory hair cells. *Nature* 449(7158):87–91.
38. Sahly I, et al. (2012) Localization of Usher 1 proteins to the photoreceptor calyceal processes, which are absent from mice. *J Cell Biol* 199(2):381–399.
39. Overlack N, Nagel-Wolfrum K, Wolfrum U (2010) The role of cadherins in sensory cell function. *Molecular and Functional Diversities of Cadherin and Protocadherin*, ed Yoshida K (Research Signpost, Scarborough, Canada), pp 259–272.
40. Mazelova J, Ransom N, Astuto-Gribble L, Wilson MC, Deretic D (2009) Syntaxin 3 and SNAP-25 pairing, regulated by omega-3 docosahexaenoic acid, controls the delivery of rhodopsin for the biogenesis of cilia-derived sensory organelles, the rod outer segments. *J Cell Sci* 122(Pt 12):2003–2013.
41. Rattner A, Chen J, Nathans J (2004) Proteolytic shedding of the extracellular domain of photoreceptor cadherin. Implications for outer segment assembly. *J Biol Chem* 279(40):42202–42210.
42. Ding JD, Salinas RY, Arshavsky RY (2015) Discs of mammalian rod photoreceptors form through the membrane evagination mechanism. *J Cell Biol* 211:495–502.
43. Volland S, et al. (2015) Three-dimensional organization of nascent rod outer segment disk membranes. *Proc Natl Acad Sci USA* 112(48):14870–14875.
44. Kremer JR, Mastronarde DN, McIntosh JR (1996) Computer visualization of three-dimensional image data using IMOD. *J Struct Biol* 116(1):71–76.
45. Slot JW, Geuze HJ, Gigengack S, Lienhard GE, James DE (1991) Immuno-localization of the insulin regulatable glucose transporter in brown adipose tissue of the rat. *J Cell Biol* 113(1):123–135.